ZIBELINE INTERNATIONAL™ PUBLISHING

ISSN: 2637-0778 (Online)
CODEN: ECRNAE

Environmental Contaminants Reviews (ECR)

DOI: http://doi.org/10.26480/ecr.01.2021.01.07

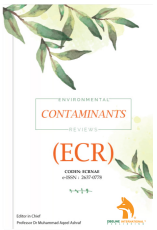

RESEARCH ARTICLE

APPRAISAL OF SNOW IN CONTEXT OF TEMPERATURE VARIATIONS IN GILGIT BASIN

Anmol Shehzadi[a*], Syed Amer Mehmood[b], Hafsa Aeman[c], Saira Batool[d]

China University of Geosciences (CUG), Wuhan, China.
Department of Space Science, University of the Punjab, New Campus, 54590, Lahore, Pakistan
State Key Laboratory of Information Engineering in Surveying, Mapping and Remote Sensing (LIESMARS), 430079, Wuhan University, China.
Centre for integrated mountain research (CIMR), university of the Punjab , Lahore
****Corresponding Author Email: shahanmol300@gmail.com***

ARTICLE DETAILS

Article History:

Received 02 October 2020
Accepted 05 November 2020
Available online 30 November 2020

ABSTRACT

The study on Appraisal of Snow in Context of Temperature Variations in Gilgit Basin was conducted to find the snow cover change over Gilgit and Hunza Rivers. Hypsometric curve for this catchment was convex upward between normalized area and elevation. Using the MODIS snow cover product classification of snow cover was done which indicate the present of snow in the catchment. Change detection technique indicates there was high level of snow cover area change during the melting period of 2011. This area of snow which melted during melting period of 2011 was 9358.762km2. There was high level of snow cover change detection appeared in the melting period of 2011, 2012 and 2015 along the Gilgit-Hunza Rivers. The minimum snow area change was observed in 2014 during the melting period. During this year snow melting was observed with low level of change detection. Besides there was also low level of snow cover change detection observed in 2013 melting period. There was decreasing trend in snow cover change appeared in this basin.

KEYWORDS

Hypsometric curve, catchment, normalized, elevation, MODIS, Change detection.

1. INTRODUCTION

Snow is a porous, permeable aggregate of ice grains (Bader, 1962). Snow crystals nucleate and begin their growth in clouds where the temperature is below 0◦C. Snow crystals can occur in a variety of relatively flat hexagonal or six sided shapes however, they can also occur as elongated columns and needles. Differences in snow crystals are a result of variations in the temperature and humidity of the atmosphere at the time of their formation and the action of the wind during their descent to the ground (Male, 1980). As a result, there is a myriad of possible shapes that can form depending primarily on the cloud temperature at the time the water vapor freezes. Freshly fallen snow almost immediately begins to compact and metamorphose, initially preserving the original shape of the snow crystal. The constant jostling and rubbing of crystals against each other cause protuberances to become chipped and broken. As the snow settles under its own weight, melts and refreezes, and is buffeted by the wind, individual crystals are further altered such that after a few days they have little resemblance to their original shape. A seasonal snowpack might have grain radii ranging from 0.1 to 0.5mm throughout the season. In the absence of a temperature gradient in the snowpack, snowflakes undergo "destructive metamorphism" and become more rounded over time, with typically slower growth rates being more characteristic of the more-rounded crystals. "Constructive metamorphism," when large grains grow at the expense of small grains, occurs when there is a thermal and vapor gradient in the snowpack and snow grains at the base of the pack grow at the expense of smaller grains, hence the crystals develop distinctive shapes (Colbeck, 1982). Dry snow will metamorphose into large depth hoar grains when subjected to a strong temperature gradient, and grain growth and dry-snow metamorphism control the movement and redistribution of mass, chemical species, and isotopes in the snowpack (Sturm and Benson, 1997). Depth-hoar crystals may grow to 1cm in size (Trabant and Benson, 1972).

1.1 Types of Snow

Early attempts to measure snow albedo remotely were conducted from aircraft (Bauer and Dutton, 1962; Hanson and Viebrock, 1964; McFadden and Ragotzkie, 1967; Salomonson and Marlatt, 1968; Dirmhirn and Eaton, 1975). More recently, however, detailed field, aircraft, and satellite studies have been undertaken to derive quantitative measurements of snow reflectance and albedo (Steffen, 1987; Hall et al., 1989; Duguay and LeDrew, 1992; Winther, 1993; Knap and Oerlemans, 1996; Stroeve et al., 1997; Winther et al., 1999; Greuell et al., 2002). Some researchers have measured the albedo of snow-covered lands using satellite data on a hemispheric scale (Kukla and Robinson, 1980; Robock, 1980; Robinson and Kukla, 1985; Robinson et al., 1992; Robinson, 1993). Both constructed basinwide albedo maps and observed differences in the timing of the melt between years (Robinson et al., 1986; Scharfen et al., 1987).

Robinson and Kukla used Defense Meteorological Satellite Program (DMSP) imagery (spectral range – 0.4–1.1μm) to derive a linear relationship between the brightest snow covered arctic tundra and the darkest snow-covered forest, which were assigned Albedo of 0.80 and

Quick Response Code	Access this article online	
	Website: www.contaminantsreviews.com	DOI: 10.26480/ecr.01.2021.01.07

Cite the Article: Anmol Shehzadi, Syed Amer Mehmood, Hafsa Aeman, Saira Batool (2021). Appraisal Of Snow In Context Of Temperature Variations In Gilgit Basin. *Environmental Contaminants Reviews, 4(1): 01-07.*

0.18, respectively (Robinson and Kukla, 1985). Scene brightness was then converted to surface albedo by linear interpolation. The surface brightness is a function of the type and density of vegetation and the depth and age of snow (Robinson and Kukla, 1985). In deriving albedo, atmospherically corrected MODIS surface reflectance in individual MODIS bands for snow-covered pixels located in non-forested areas are adjusted for anisotropic scattering effects using a discrete ordinate radiative transfer (DISORT) model and snow optical properties. Currently, in the algorithm, snow-covered forests are considered to be Lambertian reflectors. The adjusted spectral albedos are then combined into a broadband albedo measurement using a narrow-to broadband conversion scheme developed specifically for snow by Shunlin Liang (written communication, 2003) (Liang, 2000; Klein and Stroeve, 2002).

Nevertheless, in view of the importance of snowmelt for the Indus Basin, an accurate quantification of its distribution pattern and20 its climatic properties are essential. Additionally, snow cover assessment is required for the calibration/validation of distributed hydrological models, as well as for the seasonal forecast of the freshwater supplies. A similar snow cover trend has also been observed during 2000–2008 (Konz et al., 2010). During 2000–2010, though some regional anomalies do exist (Immerzeel et al., 2009; Gurung et al., 2011). In contrast, UIB experiences unique signatures of climate change, featuring cooling temperatures and increasing precipitation (Fowler and Archer, 2005b). Satellite remote sensing has proven useful tool for real-time, year-round and large spatial coverage for monitoring and process studies over vast, rugged and remote areas (Konig et al., 2001). The divergent medium resolution satellite sensors, e.g., Landsat MSS and TM have been used for the mapping of snow cover area over drainage basins (Dozier et al., 1981; Rango and Martinec, 1982; Dozier, 1984, 1989). According to Zhen and Li Areal and spatial distribution of snow and ice cover in alpine regions vary significantly over time, due to seasonal and inter-annual variations in climate (Zhen and Li, 1998).

2. Study Area and Datasets

2.1 Topography of Study Area

The total basin area is 200677 km2 and the length of the river upstream the dam is approximately 1125 km. The upper Indus basin includes the Hunza, Gilgit, Shigar and Shyok sub-basins. The altitude of the basin ranges from 335 m to 8238m and as a result, the climate within the basin varies greatly. The Gilgit River is situated at high altitudes in the Himalaya-Karakorum-Hindu Kush (HKH) region. The present study area lies between latitude 35°46´05 N to 36°51´16´´N and longitude 72°25´02´´E to 74°19´25 E. The precipitation lapse rate between low (1,460 m) and high (3,150 m) altitude climatic stations varies from season to season. In summer (April to June) it varies from 0.057 mm/100 m to 0.0002 mm/100 m. In winter, the value of precipitation lapse rate is higher in December (about 0.76 mm/100 m). This area falls in the cold desert climatic regime. The average elevation of the Gilgit catchment is about 3,997 m. The southern part of the catchment receives a maximum amount of rainfall of about 1,000 mm/year, while the amount of rainfall in agricultural areas is less than 500 mm/ year. The broad tract of the Gilgit River receives about >125 mm/year of rainfall.

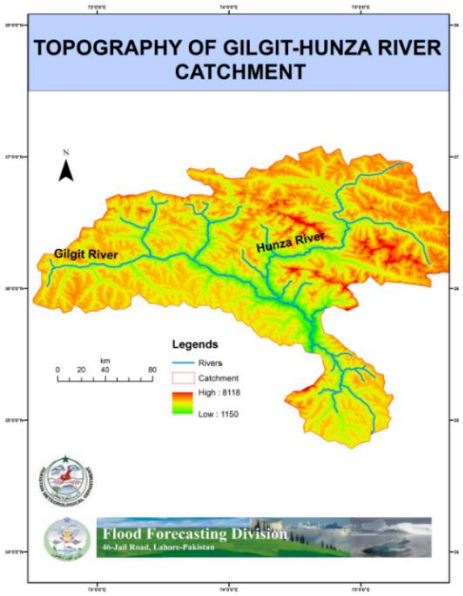

Figure 1: Topography of Gilgit- Hunza Rivers Catchment

The largest part of the basin (90%) is in the rain shadow of the Himalayas and not effected by the summer monsoon. Low intensity winter and spring precipitation originating from western low-pressure systems are the primary source of water.

2.1.1 Hydrometeorology

The Surface Water Hydrology Project of the Water and Power Development Authority (SWHP–WAPDA) carries out the stream flow measurements in Pakistan, with the earliest observations dating from 1960. A 33-year database of daily discharge covering the period of 1970–2008 (with a missing data period for 1974–79) for the Gilgit River gauged at the Gilgit hydrometric station was available for this study. Meteorological data of daily mean temperatures and daily total precipitation over 14 years (1995–2008) for two high-altitude Automatic Weather Stations (AWS), Ushkor and Yasin was provided by the WAPDA, and similar data over a ~62-year time period (1951–2012) from two valley stations, Gilgit and Gupis was provided by the PMD (Pakistan Meteorological Department). The flow direction and flow accumulation for this basin

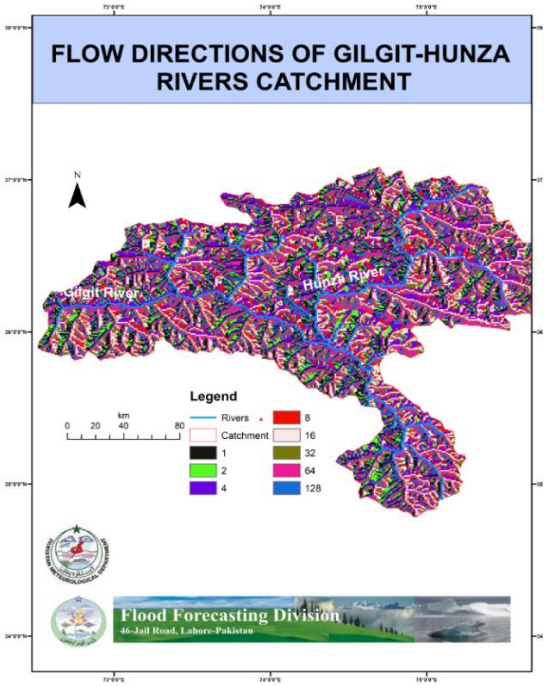

Figure 2: Flow Direction Gilgit- Hunza Rivers Catchment

2.2 Datasets

2.2.1 Modis

We have chosen the MODIS daily snow products from both Terra and Aqua (MODand MYD-10A1) Version 5for the period 2001–2012 for our anal-20 years, available at 500m resolution (Hall et al., 2006). The MODIS snow cover products have been generated through the automated snow-mapping procedure using bands 1 (0.659μm), 2 (0.865μm), 4 (0.555μm) and 6 (1.64μm). Normalized difference snow index (NDSI) using bands 4 and 6 is used to detect snow as it has high reflectance value in visible band (band 4) and low reflectance value in the short-wave infrared band2 (Hall et al., 1995). A surface temperature filtering has been included in the version 5 of the snow products in order to prevent mapping of the warm as snow, their spectral features similar to the snow (Riggs et al., 2006).

2.2.2 Aster Dem

Digital Elevation Models or DEMs are increasingly becoming the focus of attention within the larger realm of digital topographic data due to the fundamental nature of the data, and knowledge to the data they represent. The precision of DEM in simulating the true terrestrial parameters of elevation, slope and aspect improved significantly the quality and caliber of knowledge in numerous applications in earth, environmental and engineering sciences. A DEM provides a digital representation of a portion of the earth's surface terrain over a two-dimensional surface (UNEP/GRID) A DEM is an ordered array of numbers that represents the spatial distribution of elevations above some arbitrary datums in the landscape (Meijerink et al., 1994).

3. METHODS AND MATERIAL

3.1 Supervised Classification

In supervised classification the user or image analyst "supervises" the pixel classification process. The user specifies the various pixel's values or spectral signatures that should be associated with each class. This is done by selecting representative sample sites of known cover type called Training Sites or Areas. The computer algorithm then uses the spectral signatures from these training areas to classify the whole image. Ideally the classes should not overlap or should only minimally overlap with other classes. In ENVI there are three different classification algorithms you can choose from in the supervised classification procedure.

3.2 Maximum Likelihood

Assumes that the statistics for each class in each band are normally distributed and calculates the probability that a given pixel belongs to a specific class. Each pixel is assigned to the class that has the highest probability (that is, the maximum likelihood). This is the default.

3.3 Minimum Distance

Uses the mean vectors for each class and calculates the Euclidean distance from each unknown pixel to the mean vector for each class. The pixels are classified to the nearest class.

3.4 Mahalanobis Distance

A direction-sensitive distance classifier that uses statistics for each class. It is similar to maximum likelihood classification, but it assumes all class covariance are equal, and therefore is a faster method. All pixels are classified to the closest training data.

3.5 Spectral Angle Mapper

SAM is a physically-based spectral classification that uses an n-Dimension angle to match pixels to training data. This method determines the spectral similarity between two spectra by calculating the angle between the spectra and treating them as vectors in a space with dimensionality equal to the number of bands.

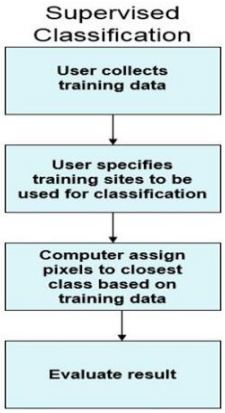

Figure 3: Supervised classification scheme

3.6 Training Sites

Training sites are areas that are known to be representative of a particular land cover type. The computer determines the spectral signature of the pixels within each training area, and uses this information to define the mean and variance of each of the classes. Preferably the location of the training sites should be based on field collected data or high-resolution reference imagery. It is important to choose training sites that cover the full range of variability within each class to allow the software to accurately classify the rest of the image. If the training areas are not representative of the range of variability found within a particular land cover type, the classification may be much less accurate. Multiple, small training sites should be selected for each class. The more time and effort spent in collecting and selecting training site the better the classification results.

4. RESULTS AND DISCUSSION

3.1 Hypsometric Curve Analysis

Hypsometry means relative proportion of an area at different elevations within a region and hypsometric curve depicts distribution of area with respect to altitude. There is 7114m and 1227m maximum and minimum elevation peaks in this catchment. The catchment area was 384.89 km2. Using ASTER data, the hypsometric parameters for this catchment was calculated. Figure 4 is the hypsometric curve for the Gilgit- Hunza rivers catchment. This curve is convex upward indicating that this basin is rather older basin.

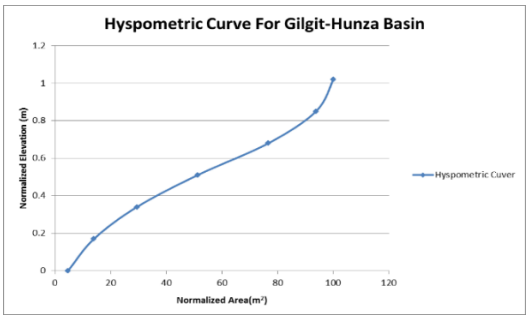

Figure 4: Elevation – area curve for Gilgit - Hunza basin

3.2 Snow Cover Area In 2010 And 2011

The total snow cover area at the start of melting period was 1853.2332km^2 which at the end of melting period becomes 4.374km^2. There was total of 1848.8592km^2 area melted during snow melting period of 2010 (Figure 5). In the start of melting period maximum snow cover was over the Gilgit River and its surrounding glaciers. The snow cover was less over Hunza River in this period (Figure 6). Snow cover change detection of Gilgit-Hunza Rivers basin indicates there are snow cover dominantly change during the snow.

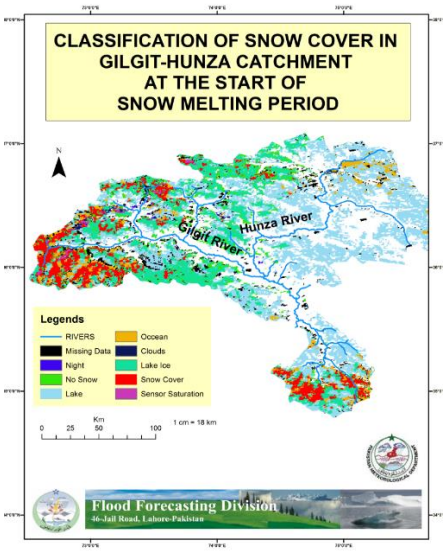

Figure 5: Snow cover classification using MODIS product at the start of snow melting period of 2010 over Gilgit-Hunza basin

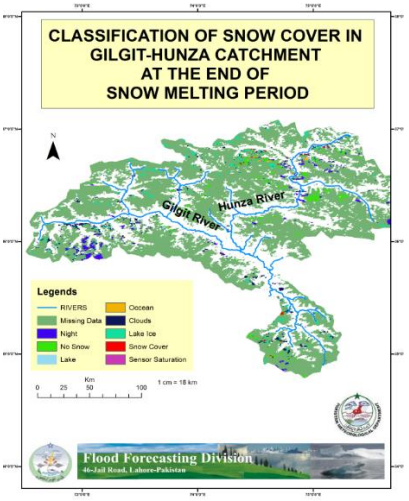

Figure 6: Snow cover classification using MODIS product at the end of snow melting period of 2010 over Gilgit-Hunza basin

Moreover, in 2011 melting year of snow cover was uniformly distributed in the Gilgit-Hunza Rivers basin. At the start of melting period total snow cover area was 9363.1356km^2 which at the end of melting period reduce to 4.374km^2 (Figure 9). In this year maximum area of snow was melted which figured out to be 9358.7616km^2 in basin (Figure 7). Snow cover change detection technique reveal that there very strong change in snow cover appeared in melting period of 2011. Glaciers along the Gilgit-Hunza Rivers facing high level of snow cover change during this melting period of the snow as shown in the Figure 9.

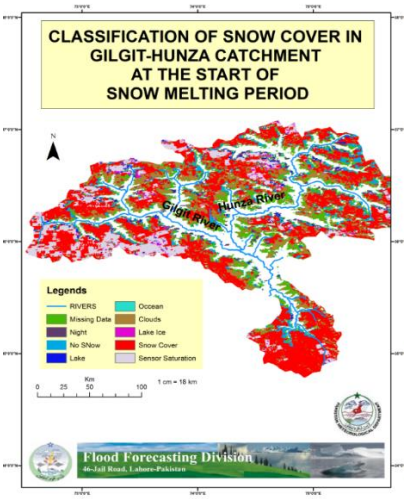

Figure 7: Snow cover classification using MODIS product at the start of snow melting period of 2011 over Gilgit-Hunza basin

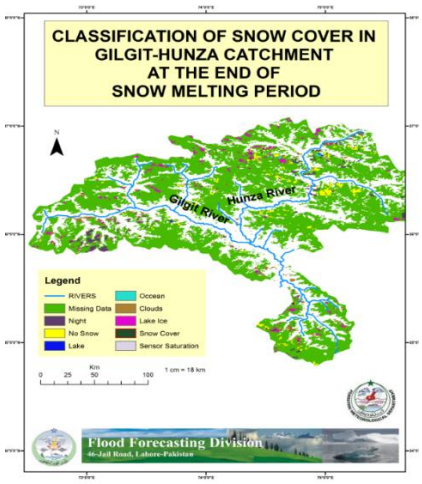

Figure 8: Snow cover classification using MODIS product at the end of snow melting period of 2011 over Gilgit-Hunza basin

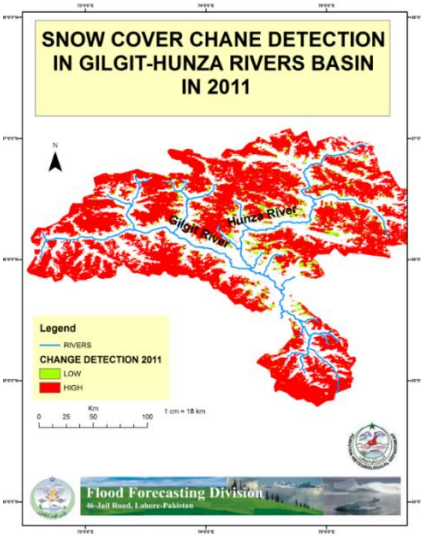

Figure 9: Snow cover change detection for the snow melt period of 2010 in Gilgit-Hunza Rivers basin

4.3 Snow Cover Area In 2012 And 2013

There was less snow cover at the start of snow melting period over the catchment. There some pockets of Gilgit River which filled with snow at the start of melting period (Figure 10). At the end of melting period when snow totally melted in the catchment. There was 4653.7857km^2 was melted in this year. Snow cover change detection technique indicates high level of snow melting during this year. Glaciers along the Gilgit-Hunza Rivers highly melted during the melting period contribute to high runoff in these rivers (Figure 10-12)

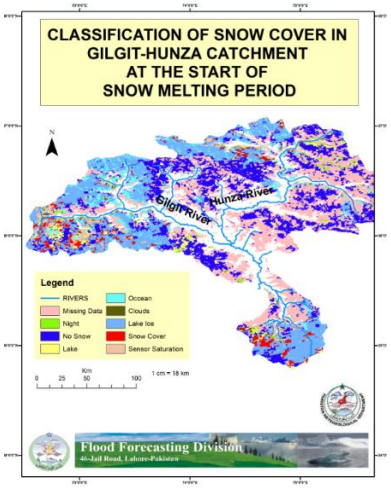

Figure 10: Snow cover classification using MODIS product at the start of snow melting period of 2012 over Gilgit-Hunza basin

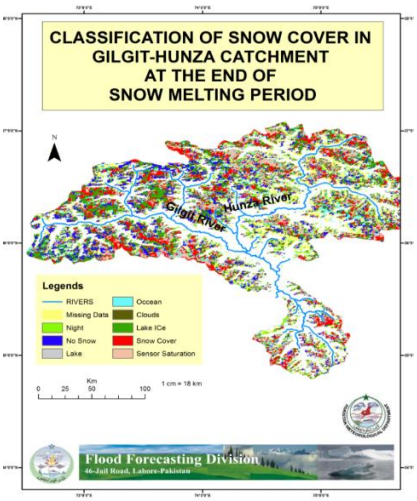

Figure 11: Snow cover classification using MODIS product at the end of snow melting period of 2012 over Gilgit-Hunza basin

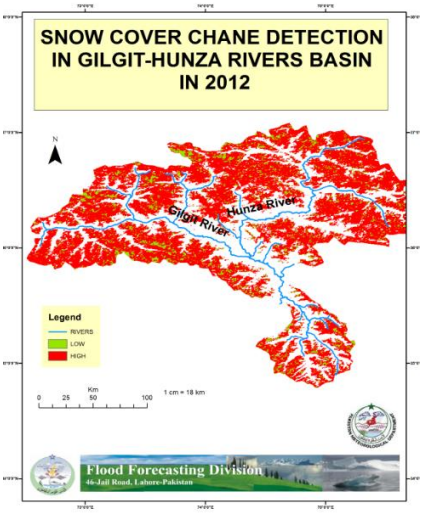

Figure 12: Snow cover change detection for the snow melt period of 2012 in Gilgit-Hunza Rivers basin

4.4 Snow Cover In 2013 And 2014

At the start of melting period 1015.8876km² of snow was found in the catchment (Figure 13). There were some glaciers around the Gilgit River contain snow cover while the Hunza River has no snow cover at the start of melting of 2013(Figure 13). At the end of melting period the area of snow becomes 1.1826km² after 1014.705km² reducing. This melted area becomes contribute to runoff of Gilgit River (Figure 14). Change detection during this melting period indicates low level of snow melting along the Gilgit-Hunza Rivers. In this year very small change was detect in snow cover during melting period (Figure 15).

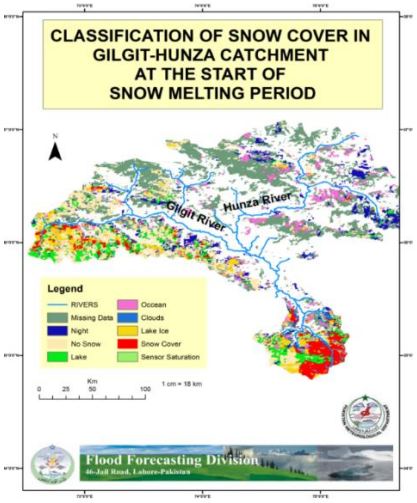

Figure 13: Snow cover classification using MODIS product at the start of snow melting period of 2013 over Gilgit-Hunza basin

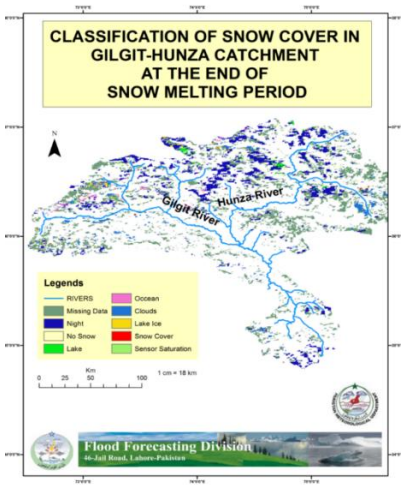

Figure 14: Snow cover classification using MODIS product at the end of snow melting period of 2013 over Gilgit-Hunza basin

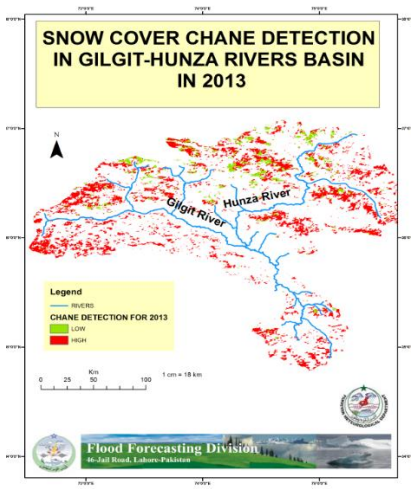

Figure 15: Snow cover change detection for the snow melt period of 2013 in Gilgit-Hunza Rivers basin

Moreover, at the start of 2014 the melting period, some pockets were filled with snow in basin (Figure 16). The total area of snow at the start of period was 327.9276km² which was the minimum area ever appeared in this research work. In this year minimum area of catchment was cover with snow and minimum also melted and contribute toward runoff of rivers (Figure 19). Very small change in snow cover area was detect during this melting year. Very small pockets along the Gilgit-Hunza Rivers indicate low level of snow melting (Figure 20)

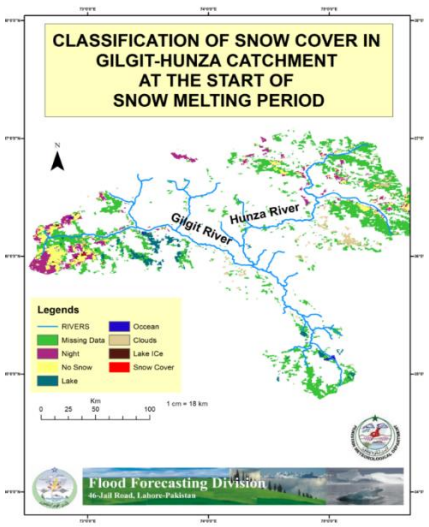

Figure 16: Snow cover classification using MODIS product at the start of snow melting period of 2014 over Gilgit-Hunza basin

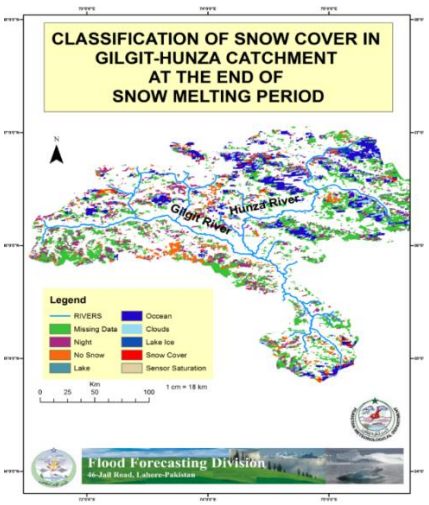

Figure 17: Snow cover classification using MODIS product at the end of snow melting period of 2014 over Gilgit-Hunza basin

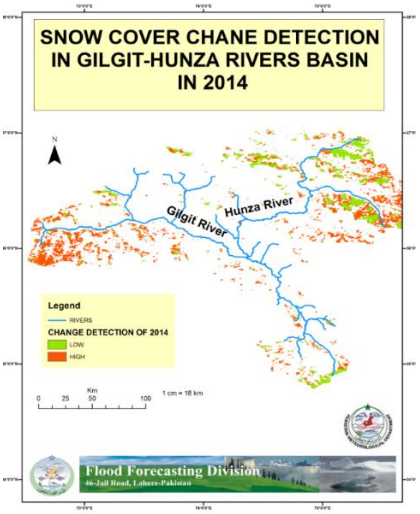

Figure 18: Snow cover change detection for the snow melt period of 2014 in Gilgit-Hunza Rivers basin

4.5 Snow Cover Area In 2015

The total area of snow cover in catchment was 1277.9676km² at the start of melting period. Mostly Gilgit and Hunza Rivers was surrounded by snow cover (Figure 19) while at the end of melting period 60.9201km²area in the catchment was cover with snow (Figure 20). High level of snow cover change detection was observed in the basing during this melting period (Figure 19). The summary of snow cover change detection calculated over this basin of Gilgit and Hunza Rivers.

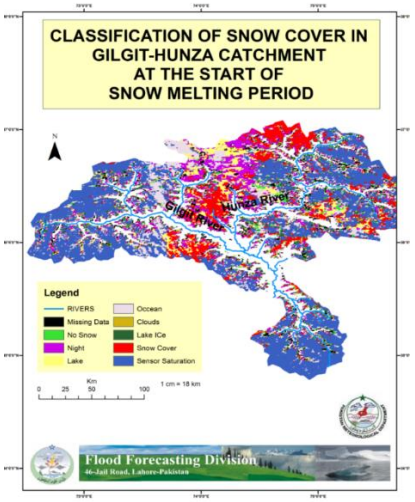

Figure 19: Snow cover classification using MODIS product at the start of snow melting period of 2015 over Gilgit-Hunza basin

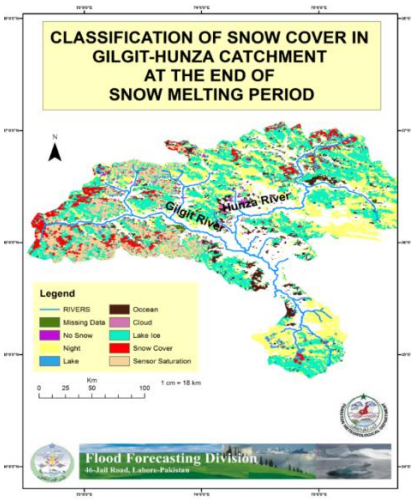

Figure 20: Snow cover classification using MODIS product at the end of snow melting period of 2015 over Gilgit-Hunza basin

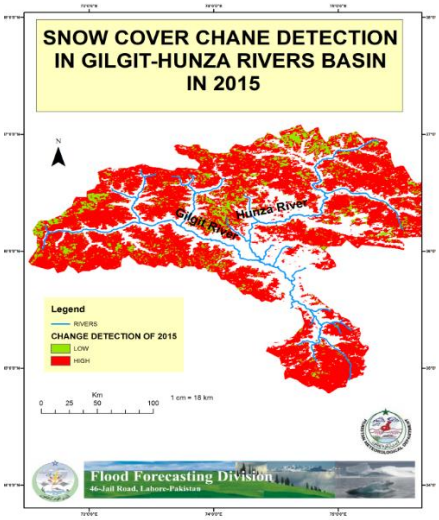

Figure 21: Snow cover change detection for the snow melt period of 2015 in Gilgit-Hunza Rivers basin

4.6 Trend Of Snow Cover Change In Gilgit-Hunza Rivers Basin

The summary of change detection in snow cover area during the melting period of 2010 to 2015 was given in Table 1. There was deceasing trend found in snow cover change from 2010 to 2015. This trend was linear in nature and giving overall lowering of snow cover area in the basin (Figure 22).

Table 1: Summary of snow cover change detection during the snow melting period 2010 to 2015

Year	Start of Melting(Km2)	End of Melting (Km2)	Area Melted (km2)
2010	1853.2332	4.374	1848.8592
2011	9363.1356	4.374	9358.7616
2012	4916.7846	262.9989	4653.7857
2013	1015.8876	1.1826	1014.705
2014	327.9276	15.4872	312.4404
2015	1277.9676	60.9201	1217.0475

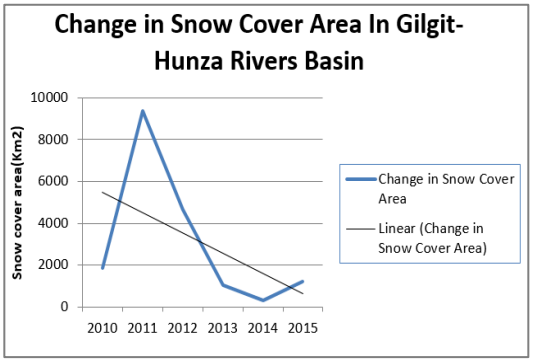

Figure 22: Deceasing trend in snow cover over Gilgit-Hunza River basin during snow melting period of 2010 to 2015

5. Conclusion

Based upon critical checks and evaluations it was concluded that snow cover plays a major role in the runoff of Gilgit and Hunza Rivers. Snow cover area of 9358.762km² was melted during the snow melting period of 2011. This change in area was highest among the 2010-2015 melting periods. Snow cover classifications indicates mostly snow exited over glaciers of Gilgit and Hunza Rivers which melted till the end of melting period. Minimum snow cover change observed in 2014 snow melting period. On this year 312.4404km² area was observed melted during melting period. This melted area was minimum among all the melted snow cover areas of 2010 to 2015. Mostly the glaciers around these rivers contain less snow content and less contribution of snow melt. The hypsometric curve was convex upward and there was decreasing trend was observed in the change of snow cover are in this basin during the melting periods.

Recommendations

This study was conduct on the basin of MODIS satellite snow cover area product. Snow cover change always contributes to flows of rivers. Unfortunately, there was not runoff data available over Gilgit and Hunza Rivers that why the effect of this snow cover area change to runoff was not investigated. It is recommended for further studies to observed the effect of snow cover change to runoff of these rivers.

References

Armstrong, R.L., Brodzik, M.J., 2001. Recent northern hemisphere snow extent: a comparison of data derived from visible and microwave satellite sensors. Geophysical Research Letters, 28 (19), Pp. 3673–3676.

Bader, H., 1962. The Physics and Mechanics of Snow as a Material, Cold Regions Research and Engineering Laboratory: Hanover, Report II-B, Pp. 1.

Bhambri, R., Bolch, T., Kawishwar, P., Dobhal, D.P., Srivastava, D., Pratap, B., 2013. Heterogeneity in glacier response in the upper Shyok valley, northeast Karakoram. The Cryosphere, 7, Pp. 1385–1398, doi:10.5194/tc-7-1385-2013.

Bolch, T., Kulkarni, A., Kääb, A., Hugget, C., Paul, F., Cogley, J. G., Frey, H., Kargel, J.S., Fujita, K., Scheel, M., Bajracharya, S., Stoffel, M., 2012. The

state and fate of Himalayan glaciers. Science, 336, Pp. 310–314.

Colbeck, S.C., 1982. An overview of seasonal snow metamorphism, Reviews of Geophysics and Space Physics, 20 (1), Pp. 45–61.

Diodato, N., Bellocchi, G., Tartari, G., 2012. do Himalayan areas respond to global warming? Int. J. Climatol., 32, Pp. 975–982.

Dozier, J., Painter, T.H., 2004. Multispectral and hyperspectral remote sensing of alpine snow properties. Annual Reviews of Earth and Planetary Science, 32, Pp. 465–494.

Gardelle, J., Berthier, E., Arnaud, Y., 2012. Slight gain of mass by Karakoram glaciers in the early 21st century, Nat. Geosci., 5, Pp. 322–325.

Gurung, D.R., Amarnath, G., Khun, S.A., Shrestha, B., Kulkarni, A.V., 2011. Snow-cover mapping and monitoring in the HinduKush-Himalayas, ICIMOD, Kathmandu.

Gurung, D.R., Amarnath, G., Khun, S.A., Shrestha, B., Kulkarni, A.V., 2007. Snow-cover mapping and monitoring in the HinduKush-Himalayas, ICIMOD, Kathmandu, 2011. Hall, D. K. and Riggs, G. A.: Accuracy assessment of the MODIS snow products, Hydrol. Process., 21, Pp. 1534–1547, doi:10.1002/hyp.6715, 2007

Hasson, S., Lucarini, V., Pascale, S., Böhner, J., 2013. Seasonality of the hydrological cycle in major South and Southeast Asian River Basins as simulated by PCMDI/CMIP3 experiments,10 Earth Syst. Dynam. Discuss., 4, Pp. 627–675, doi:10.5194/esdd-4-627-2013.

Immerzeel, W.W., Droogers, P., de Jong, S.M., Bierkens, M.F.P., 2009. Large-scale monitoring of snow cover and runoff simulation in Himalayan river basins using remote sensing, Remote Sens. Environ., 113, Pp. 40–49.

K¨onig, M., Winther, J.G., and Isaksson, E., 2001. Measuring snow and glacier ice properties from satellite. Reviews of Geophysics, 39 (1), Pp. 1–27.

Knap, W.H., Oerlemans, J., 1996. The surface albedo of the Greenland ice sheet: satellite-derived and in situ measurements in the Søndre Strømfjord area during the 1991 melt season. Journal of Glaciology, 42 (141), Pp. 364–374.

Konz, M., Finger, D., Buergi, C., Normand, S., Immerzeel, W.W., Merz, J., Girirah, A., Burlando, P., 2010. Calibration of a distributed hydrological model for simulations of remote glaicerised Himalayan catchments using MODIS snow cover data, Global Change: Facing Risks and Threats to Water Resources (Proc. Of the Sixth World FRIEND Conference, Fez, Morocco,15 IAHS Publ., 340, Pp. 465–473.

Male, D.H., 1980. The seasonal snowcover. In Dynamics of Snow and Ice Masses, Colbeck S. (Ed.), Academic Press: New York, Pp. 305–395.

Moody, E., King, M., Schaaf, C., Hall, D., Platnick, S., 2007. Northern Hemisphere five-year average (2000--2004) spectral albedos of surfaces in the presence of snow: Statistics computed from Terra MODIS land products. Remote Sensing of Environment, 111 (2), Pp. 337-345.

Robinson, D.A., Frei, A., 2000. Seasonal variability of northern hemisphere snow extent using visible satellite data. Professional Geographer, 51, Pp. 307–314.

Salomonson, V.V., Appel, I.L., 2004. Estimating the fractional snow covering using the normalized difference snow index. Remote Sensing of Environment, 89, Pp. 351–360.

Scharfen, G.R., Hall, D.K., Khalsa, S.J.S., Wolfe, J.D., Marquis, M.C., Riggs, G.A., McLean, B., 2000. Accessing the MODIS snow and ice products at the NSIDC DAAC. Proceedings ofIGARSS'00, Honolulu, Pp. 2059–2061.

Stroeve, J., Nolin, A., Steffen, K., 1997. Comparison of AVHRR-derived and in situ surface albedo over the Greenland Ice sheet. Remote Sensing of Environment, 62, Pp. 262–276.

Trabant, D., Benson, C., 1972. Field experiments on the development of depth hoar. Studies in Mineralogy and Precambrian Geology, Doe B.R. and Smith K.K. (Eds.), Geological Society of America Memoir, 135, Pp. 309–322.

Trabant, D., Benson, C., 1972. Field experiments on the development of depth hoar. Studies in Mineralogy and Precambrian Geology, Doe B.R. and Smith K.K. (Eds.), Geological Society of America Memoir, 135, Pp. 309–322.